DOI: 10.1002/ ((please add manuscript number))
Article type: Full Paper

Enhanced Hetero-Junction Quality and Performance of Kesterite Solar Cells by Aluminum Hydroxide Nanolayers and Efficiency Limitation Revealed by Atomic-resolution Scanning Transmission Electron Microscopy

*Haibing Xie,*Yudania Sánchez,Pengyi Tang,Moisés Espíndola-Rodríguez,Maxim Guc, Lorenzo Calvo-Barrio, Simon López-Marino,Yu Liu, Joan R. Morante, Andreu Cabot,Victor Izquierdo-Roca, Jordi Arbiol, Alejandro Pérez-Rodríguez, and Edgardo Saucedo**

Dr. H. Xie, Dr. Y. Sánchez, Dr. P. Tang, Dr. M. Espíndola-Rodríguez, Dr. M. Guc, Dr. S. López-Marino, Dr.Y. Liu, Prof. J. R. Morante, Prof. A. Cabot, Dr. V. Izquierdo-Roca, Prof. A. Pérez-Rodríguez, Dr. E. Saucedo
Catalonia Institute for Energy Research (IREC)
Jardins de les Dones de Negre 1, 2a, Sant Adrià del Besòs
Barcelona, 08930, Spain
E-mail: xhaibing00@outlook.com, esaucedo@irec.cat

Dr. P. Tang, Prof. J. Arbiol
Catalan Institute of Nanoscience and Nanotechnology (ICN2)
CSIC and Barcelona Institute of Science and Technology (BIST)
Campus UAB
Bellaterra, Catalonia, 08193, Spain

Prof. L. Calvo-Barrio
Centres Científics i Tecnològics de la Universitat de Barcelona (CCiTUB)
Lluís Solé i Sabarís 1-3
Barcelona, 08028, Spain

Prof. L. Calvo-Barrio, Prof. A. Pérez-Rodríguez
Institute for Nanoscience ans Nanotechnology of the University of Barcelona (IN2UB)
Departament d'Electrònica
Universitat de Barcelona
Barcelona, 08028, Spain

Prof. J. Arbiol, Prof. A. Cabot
Institució Catalana de Recerca i Estudis Avançats (ICREA)
Pg. Lluís Companys 23
Barcelona, 08010, Spain

Keywords: kesterite, $Al(OH)_3$ nanolayer, thin film solar cell, interface passivation, Atomic-resolution Scanning Transmission Electron Microscopy

A strategy for interface engineering of hetero-junction in kesterite solar cells by using $Al(OH)_3$ is demonstrated. The hydroxide nanolayers are prepared via a facile and fast wet chemical route, based on an aqueous solution of aluminum chlorides and thioacetamide. Considerable enhancement of open circuit voltage (V_{oc}) (30-60 mV) and fill factor (FF) (10-20%) after this chemical treatment are observed, achieving a champion conversion efficiency of 9.1% and a champion FF of 70% (among the best FF in kesterite solar cells). The functional mechanism is systematically studied by current-voltage, capacitance-voltage, temperature dependence of current-voltage and photoluminescence measurements, which reveal that $Al(OH)_3$ nanolayers can effectively reduce the interface recombination and largely improve the shunt resistance. Furthermore, atomic resolution high angle annular dark field scanning transmission electron microscopy (HAADF-STEM) evidences the epitaxial relationship of $Al(OH)_3$ with kesterite and CdS, indicating the benign and effective interface passivation by this chemical treatment. Finally, based on HAADF-STEM and electron energy loss spectroscopy (EELS) mappings, insights into the efficiency limiting and beneficial factors for CZTSSe solar cells, as well as suggestions to further improve both the bulk and related interfaces are presented.

1. Introduction

Kesterite $Cu_2ZnSn(S,Se)_4$ (CZTSSe) solar cells have captured the interest of the scientific community in the last decade due to their earth-abundant and low toxic constituent elements. CZTSSe solar cells are considered as a major candidate to replace $Cu(In,Ga)Se_2$ (CIGS) solar cells, which have raised concerns over the supply of indium and gallium due to production constrains, competing market forces, and uncertain reserve constraints, when aiming at a future mass production in the TW level.[1,2] Nevertheless, kesterites are still far below their chalcopyrite counterpart CIGS in terms of solar cell conversion efficiency (12.6% for record

CZTSSe versus 22.9% for record CIGS solar cells).[3,4] Among the reasons, a large open circuit voltage (V_{oc}) deficit ($E_{og}/q - V_{oc}$, E_{og} is the optical band gap, q is the elementary charge) is frequently reported for kesterite solar cells, with lowest values around 600 mV in contrast with around 400 mV in highly efficient CIGS solar cells.[3,5-8] Although it is widely accepted that bulk defects including band tailing are the main causes for V_{oc} deficit in kesterite solar cells,[9-12] the CZTSSe/CdS interface recombination is usually reported even in high efficiency devices, including the current record kesterite solar cell.[3,13-16] Interface recombination has several origins, e.g., a "cliff" like conduction band offset (CBO) of CZTSSe/CdS,[17-19] secondary phases on the surface,[20,21] and lattice mismatch between buffer layers and absorbers, etc.[22] Apart from V_{oc} deficit, fill factor (FF) deficit (70% for the record CZTSSe versus 80% for the record CIGS solar cell) is another hurdle for kesterite solar cells, which is related to V_{oc} deficit and series and shunt resistance losses. In particular, low shunt resistance is observed frequently in solar cells, due to shunt paths caused by structural damages or defects like pinholes, trenches and stacking faults and non-coverage points of buffer layers in the interface region.[23-26]Therefore, engineering the CZTSSe/CdS interface is of key importance for kesterite solar cells and could be a reasonable and effective way to reduce V_{oc} and FF deficit for further improvement of CZTSSe solar cells efficiency.

One way to reduce the interface recombination is chemical passivation via growing a top layer binding to the dangling bonds, which is extensively applied in photovoltaic technologies, e.g., currently the most popular mono-crystalline and poly-crystalline silicon solar cells in the market achieve high conversion efficiency through SiO_x or Al_2O_3 surface/interface passivation.[27] Na_2S and $(NH_4)_2S$ solutions were reported to produce a surface passivation effect on the CZTSSe absorbers, but the V_{oc} and FF increase of the solar cells were mainly associated to the removal of ZnSe and Sn(S,Se) secondary phases.[20,21] Additionally, Wu et al. reduced interface recombination and increased the V_{oc} of CZTSSe based solar cells by introducing an ultra-thin layer of TiO_2 using atomic layer deposition (ALD) in between the

absorbers and CdS.[28] However, the conversion efficiency of the devices was only slightly improved due to a deterioration of short circuit current density (J_{sc}) and almost unaffected FF. IBM reported that ALD of Al_2O_3 nanolayers onto the surface of CZTSSe absorbers can effectively passivate the surface and largely improve the performance mainly due to the enhanced FF and J_{sc}.[29] The ALD process seems promising, but it is expensive and time consuming (minutes to hours), and thus exploring low cost alternatives is of key relevance for kesterite solar cells. In the case of CIGS solar cells, Nakada et al. reported that chemical treatment of CIGS absorbers by using aqueous solutions with group Ⅲ chlorides (Ⅲ = In, Ga, Al, Y) and thioacetamide (CH_3CSNH_2) for 10s can improve all the photovoltaic parameters of the devices.[30] The improved cell performance was attributed to the formation of very thin sulfide layers on the CIGS absorbers and/or surface passivation by S atoms. In addition, when this chemical passivation process (Ⅲ = In and/or Ga) was applied to CIGS/Zn(O,S) hetero-junction, considerable efficiency improvement was observed, due to reduced interface recombination and enhanced minority carrier lifetime.[31,32] Thus it can be inferred that research and demonstration of this chemical passivation process on CZTSSe solar cells is an interesting field to explore. Among group-Ⅲ elements, aluminum is earth abundant, low cost and non-toxic, thereby aluminium chloride ($AlCl_3$) and thioacetamide (CH_3CSNH_2) (AT) aqueous solution chemical treatment is of high interest in order to keep the materials abundance related advantage of kesterite solar cells. However, in previous works mentioned above, this particular chemical treatment was not deeply studied compared with those In and Ga related treatments. In consequence, the exact species formed during the chemical process as well as related functional mechanism, are still unknown, and thereby they require deeper investigation to allow for a possible deployment in the field of chalcogenide thin film solar cells.

In this work, we report on a wet chemical treatment of kesterite surface, based on an aqueous solution of aluminum chloride ($AlCl_3$) and thioacetamide (CH_3CSNH_2), with the aim of improving the performance of the CZTSSe solar cells by reducing the CZTSSe/CdS interface recombination. The interface passivation effect and functional mechanism of the chemical treatment on CZTSSe solar cells are discussed. Systematic characterization studies by X-ray photoelectron spectroscopy (XPS), current density-voltage curves (J-V), external quantum efficiency (EQE), capacitance-voltage (C-V), temperature dependence of J-V (JV-T) and temperature dependence of photoluminescence (PL-T) measurements, high resolution TEM (HRTEM), atomic resolution HAADF-STEM and electron energy loss spectroscopy (EELS) are included. Results show a significant enhancement of V_{oc} and FF of CZTSSe devices, due to an effective interface passivation by the epitaxial growth of $Al(OH)_3$ nanolayers, which may pave the way to reduce interface recombination and V_{oc} and FF deficit, leading to high efficiency devices in the CZTSSe field.

2. Results and discussion

2.1. CZTSSe absorbers surface after $AlCl_3$ and thioacetamide (AT) chemical treatment

XPS, SEM and XRD were performed onto the reference and AT treated samples, but no remarkable change can be found (see **Figure S1-S3**). Here the AT solution is based on 0.005 M $AlCl_3$ and 0.1 M thioacetamide and soaking time is 60s. To identify the species formed on absorber surface during the AT treatment, the AT treated CZTSSe absorber was removed from the Mo substrate by careful scraping (keeping the morphology of the surface) and dispersed in hexane for HRTEM measurements. **Figure 1** shows the HRTEM micrographs and corresponding fast Fourier transform (FFT) and inverse fast Fourier transform (IFFT) images of one representative dispersed CZTSSe absorber nanoparticle, which validates that the CZTSSe absorbers are covered with monoclinic γ-$Al(OH)_3$ (Gibbsite). This is in contrast with the results of Nakada et al., probably due to the overlapped Al and Cu peaks in XPS, as

is shown in Figure S1. The absence or low concentration of Al-S species is attributed to the high instability of Al_2S_3 in aqueous solution (e.g., reacting with H_2O to form hydroxides and H_2S).[33,34] In contrast, $Al(OH)_3$ is almost insoluble in H_2O, with solubility product constant K_{sp} equal to 1.3×10^{-33} at 25 ℃.[35]

2.2 Impact of AT chemical treatment on devices and mechanism analyses

Figure 2a shows the schematic of the AT treatment and the device architecture of CZTSSe solar cells. **Figure 2 b-e** display the optoelectronic properties of CZTSSe solar cells before and after the AT treatment. A significant enhancement of all the optoelectronic parameters except for J_{sc} is observed after the AT treatment. In average, V_{oc} and FF of the devices are improved by over 60 mV and 15%, respectively, leading to an increased efficiency from 4.3% to around 7%. **Table 1** shows the diode parameters extracted from illuminated J-V curves of the reference and AT treated CZTSSe solar cells (devices with maximum efficiency in both groups are chosen). The decrease of diode ideality factor (A) and reverse saturation current density (J_0) after the treatment indicate better p-n junction quality and CZTSSe/CdS interfacial properties. In addition, the reduced series resistance (R_s) and considerably increased shunt resistance (R_{sh}) explain the large enhancement of FF in the devices. The increment of shunt resistance could be derived from less shunt paths by the coverage of $Al(OH)_3$. The decrease of series resistance will be discussed later.

To shed more light on the impact of AT treatment, external quantum efficiency (EQE), capacitance-voltage (C-V), temperature dependence of current-voltage (JV-T) and photoluminescence (PL-T) measurements were performed onto the reference CZTSSe device and AT treated one. An increase of EQE in the range of 500-650 nm coupled with a decrease of EQE in the range of 800-1200 nm are observed after the chemical treatment (see **Figure 3a**). The optical band gaps extracted from EQE plots are 1.15 eV for both samples, confirming a lower V_{oc} deficit for the chemical treated device. Additionally, C-V measurements (see **Figure 3b**) show that after AT treatment, the carrier concentration increases from 6.7×10^{15} to $1.4\times$

10^{16} cm^{-3}, which could explain the reduction of the R_s due to the inverse dependency between resistivity and carrier concentration. In addition, the increased carrier concentration can also partially interpret the higher V_{oc}.[36] Accordingly, the space charge region (SCR) width (X_d, at zero voltage) goes down from 306 to 281 nm. Therefore, the enhancement of EQE in the short wavelength region can be attributed to better p-n junction quality (e.g., less reverse saturated current in the interface region) while the deterioration of EQE in the long wavelength region could be ascribed to a shorter SCR width, leading to a reduced effective carrier collection length. It has to be noted that, the increased EQE in 500 - 650 nm cannot be ascribed to thinner CdS layer, because the CdS absorption range is mainly in 400-500 nm range due to its band gap of 2.4 eV.

Temperature dependence of V_{oc} measurements were performed to determine the activation energy of the dominant recombination mechanism (see **Figure 3c**). The activation energy can be extracted from the vertical intercept at T = 0 K of the linear extrapolation of the plot for the temperature dependence of V_{oc}, according to the following equation:[37]

$$V_{oc} = \frac{\Phi_b}{q} - \frac{AkT}{q} \ln\left(\frac{J_{00}}{J_L}\right) \qquad (1)$$

with Φ_b as the activation energy, A the diode ideality factor, J_L the light current density, and J_{00} the prefactor dependent on the specific recombination mechanism that dominates the saturation current. Theoretically, when $\Phi_b = E_{og}$ the main recombination path is located in the absorber layer and when $\Phi_b < E_{og}$ it suggests that additional recombination like interface recombination is involved [37]. The activation energy extracted from Equation (1) increases approximately from 0.7 to 0.8 eV after chemical treatments. The activation energy for both devices are much lower than the optical band gaps (1.15 eV), indicating interface recombination is present in these devices. Nevertheless, the improved Φ_b by nearly 0.1 eV demonstrates reduced interface recombination in AT treated CZTSSe solar cells.

Figure 3d presents the photoluminescence (PL) band maximum position of the reference and AT treated CZTSSe devices as a function of temperature (PL spectra can be found in **Figure S4**). Both samples show a red shift of the band maximum up to ~ 150 K and blue shift at higher temperatures. Similar dependencies were observed previously for CZTSSe solid solutions with quasi donor-acceptor pair (QDAP) emission and detailed explanations can be found elsewhere.[38,39] It is notable that the PL peak of the AT treated sample exhibits blue shift (around 10 mV) in the whole range of temperatures with respect to the reference one. This is normally attributed to increased band gap of the absorbers. As the optical band gaps keep constant and represent the in-depth E_{og} minimum, it can be speculated that the surface band gap of the absorbers increases after the chemical process. However, the donor and acceptor defect levels detected by PL-T measurements are unaffected after AT chemical treatments (see Figure S4 for detailed PL analyses).

Therefore, V_{oc} enhancement after AT treatment can be attributed to the decrease of interface recombination as well as increased carrier concentration and surface band gap.

To further understand the impact of AT treatment on CZTSSe devices from the compositional and structural point of view, the CZTSSe/CdS interface region was characterized by atomic resolution HAADF-STEM combined with electron energy loss spectroscopy (EELS) mapping. **Figure 4** shows the EELS chemical composition maps of the front interface region of a representative AT treated device. The layout of the solar cell configuration, i.e., CZTSSe/CdS/ZnO/ITO, involving Cu and Se in the CZTSSe layer, Cd and S in the CdS layer, Zn in the ZnO layer and Sn in the ITO layer, can be easily identified, being consistent with the deposition sequence. The Al distribution is in line with the O distribution, correlating with the $Al(OH)_3$ layer. This layer has a thickness ranging from 30 to 70 nm depending on the morphology of the CZTSSe absorber surface, and overlaps with the CdS layer, probably due to the intermixing of the two layers as gibbsite is an important adsorbent with porous features[40], explaining why such an insulating layer (band gap is

around 10 eV)[41] does not significantly reduce current of the devices. It should be noted that in the CdS layer, Cu, Zn and Sn are also visible. Especially, close examination shows the coupling of the distribution of Cu and Zn, along with the relative deficiency of Sn and Se. This could be due to the removal of Sn and chalcogen from the top surface layer of CZTSSe by $(NH_4)_2S$ etching[20], rather than to the random inter-diffusion of Cu, Zn and Sn from CZTSSe absorber and window layer into CdS buffer layer. Furthermore, Cu and Zn have an inverse coupling with Al and O, e.g., the voids in the Cu and Zn distribution maps are filled with Al and O correspondingly, indicating that Al and O penetrate into the surface of CZTSSe layer. This illustrates the increase of surface band gap and carrier concentration, presumably due to Al or O substitution for Sn or anion vacancy sites, respectively.[42-44]

Additionally, atomic resolution HAADF-STEM images and corresponding FFT patterns of the CZTSSe/CdS interface region (see **Figure 5**) indicates that an interfacial gibbsite layer is formed, being consistent with the HRTEM results. Furthermore, an epitaxial relationship of $Al(OH)_3$ with CZTSSe and CdS is confirmed, which is (11-2) [201] CZTSSe || (2-10)[12-1] Al(OH)3|| (1-11)[011] CdS, due to their close plane distance of 3.25 Å, 3.29 Å and 3.36 Å. The relative orientation of these parallel planes is shown by the parallelograms on FFT patterns at the bottom of Figure 5. The details of the plane distances and angles are shown in **Table S1**. The epitaxial relationship of $Al(OH)_3$ with CZTSSe and CdS indicates the benign and effective interface passivation by gibbsite nanolayers, correlating with the reduced interface recombination and shunt paths and ultimately higher V_{oc} and FF. Another explanation for the interface recombination suppression is that $Al(OH)_3$ nanolayer could act as an insulator barrier for carrier recombination, similar to the role of Al_2O_3[45].

It should be pointed out that the gibbsite formed during the chemical process is thermodynamically stable below 300 ℃.[46] In addition, the CdS CBD process did not dissolve the $Al(OH)_3$ nanolayers, and this is due to the weak alkaline solution of the CBD process (pH = 9.5). The fact that gibbsite nanolayers can endure the harsh temperature and chemical

conditions during the fabrication process and working environment of kesterite solar cells, implies that they are suitable and compatible for the effective interface engineering of kesterite solar cells.

2.3 Optimization of AT chemical treatment

The concentration of the $AlCl_3$ and thioacetamide and soaking time were systematically studied and optimized (**Figure S5 and S6**), achieving a champion efficiency of 9.1% and a champion FF of 70% for Se-rich CZTSSe solar cells when treated for 120 s and 300 s ,respectively, with 0.01 M $AlCl_3$ and 0.1 M thioacetamide chemical combination. The reduced dispersion of optoelectronic parameters indicate more homogenous interface after AT treatment for longer soaking time. **Figure 6a** shows the optoelectronic properties of the champion device, with J_{sc} = 28.9 mA.cm^{-2}, V_{oc} = 457 mV and FF = 69.2 %. The EQE reaches nearly 90 % in the 500-600 nm range (**Figure 6b**), indicating good carrier collection in the p-n junction region. A band gap of 1.15 eV is extracted. It should be noted that neither anti-reflective coating (ARC) nor metallic grids were used, and thereby further improvement of J_{sc} and subsequently higher efficiency could be expected when introducing those elements in the solar cell architecture. Temperature dependence of V_{oc} measurement of the 9.1 % champion solar cell was performed (**Figure 6c**), which shows that the activation energy is enhanced up to 1.02 eV after optimized chemical treatments. The activation energy equals the value of the world record CZTSSe solar cell with a similar band gap[3], evidencing the substantially suppression of the interface recombination. It has to be noted that, we have applied the AT treatment (0.01 M $AlCl_3$ and 0.1 M thioacetamide, 120 s) on more efficient reference devices with an average efficiency of 8.2 %, which shows an improvement to 9.0 % in average after treatment (Figure S7).

2.4 Efficiency limitation discussion

The champion 9.1% CZTSSe solar cell in this work has comparable FF (due to the comparable R_s and R_{sh}) as that of the world record CZTSSe solar cell while still suffering substantial J_{sc} and V_{oc} loss. This could also be related to carrier recombination in the back interface or the bulk. Based on the atomic resolution HAADF-STEM and EELS mapping measurements, insights into the efficiency limiting as well as beneficial factors related to the bulk and the back interface, will be given. This information will be used as guidance for further optimization of the CZTSSe solar cells produced in this work, but in addition it might provide useful hints for the whole CZTSSe community in the quest for higher solar cell efficiency.

2.4.1 Bulk (CZTSSe)

Grain boundaries (GBs): The bulk layer is composed of large grains comparable to the size of the cross section with straight or nearly straight grain boundaries (SGBs) (see **Figure 7**). GBs can be considered as planar defects with considerable associated internal free energy.[47] Therefore, large grains with SGBs are predominantly favorable, due to the grain boundary area reduction (GBAR) and ultimately the reduction of internal free energy.[47] Based on the HAADF-STEM analysis, the misorientation angle is determined to be 33.61 ºand the rotation axis is [13-2] for the two adjacent grains analyzed in Figure 7, indicating this GB is high angle (>15º) and coincidence site lattice (CSL) GB, but not a Σ3 type GB (60 ºor near 70 º). Other measurements on different SGBs show similar results, with misorientation angles > 15 º being assigned to high angle CSL GBs. Σ3 type GBs extensively exist in chalcopyrite solar cells, appearing also as twin boundaries.[48,49] This type of GBs has low misfit and free energy and reveals less non-radiative recombination and lower mean-inner potential wells than other types of GBs.[48,49] Therefore, with respect to Σ3 type GBs, the SGBs in this sample could cause more non-radiative recombination and thus may contribute to the V_{oc} deficit.

Stacking faults (SFs): Stacking faults are clearly found in the CZTSSe bulk by the corresponding dilatation map (+9.8% deformation) and rotation map (+9.5 °rotation) via geometrical phase analysis (GPA)[50] based on (020) planes of CZTSSe reflections, as shown in **Figure 8**. The stacking fault shown in this figure expands from the top layer of CZTSSe to the interface, which could be caused by Cu/Sn disorder (i.e., Cu_{Sn} and Sn_{Cu}), as supported by the forbidden peaks in the XRD patterns located at around 26.5 ºto the left shoulder of (112) peak of kesterite phase and theoretical simulation (see **Figure S8**).[51] This might mean that the stacking faults in the bulk are accumulating charged deep defects,[52] leading to the bulk recombination and ultimately the loss of V_{oc} and J_{sc}. In addition, the stacking faults might also act as shunt paths when Na is accumulated, as suggested in silicon solar cells.[53]

Secondary phases/inclusions: Sn-S-O secondary phases/inclusions are detected at the back region of the absorbers (see **Figure S9**), and they might cause band gap/electrostatic potential fluctuations, leading to V_{oc} loss. The Sn-S-O secondary phases/inclusions in the bulk could be related to excess of Sn in the metallic precursors or local composition inhomogeneity or fluctuation during thermal treatments. Thus, fine tuning of Sn during the precursor preparation and promoting the intermixing of the precursors elements (e.g., by pre-alloying and homogenization) could be plausible solutions. It has to be noted that secondary phases are common issues in kesterite solar cells, including the current world record device.[3] Their appearance is strongly related to the extremely narrow single phase existence domain in the phase diagram,[54,55] non-stoichiometry composition (e.g., Cu-poor Zn-rich) applied for high efficiency devices[56,57] and non-equilibrium conditions during thermal treatments (e.g., low annealing temperature with respect to the melting point, short holding time and discontinuous supply of chalcogen sources).

Voids: Voids with the size of several hundreds of nanometers are located in the back region of the bulk and near the CZTSSe/Mo interface (see Figure S8). In fact, voids are reported to be present in the bulk especially in the absorber/Mo interface region of CIGS and CZTSSe solar

cells, including the record kesterite solar cell.[3, 58-61] The origin is assumed to be related to Kirkendall effect due to the different diffusion rate of constituents, e.g., Cu has higher diffusivity than other elements and tends to diffuse through the bulk to the surface to react with S/Se, thus leaving behind vacancies that facilitate other elements diffusion to the surface, and finally voids are formed in the bulk or in the absorber/Mo interface.[59,62-64] Additionally, for kesterite solar cells, the detrimental reaction between CZTSSe and Mo and the volatile Sn chalcogenides loss during elevated reaction temperatures are also considered as possible reasons.[65,66] The voids near the CZTSSe/Mo interface clearly influence the mechanical properties like adhesion between absorbers and Mo. However, the impact of voids on the performance of solar cells is still an open question. Some researchers reported that the voids could reduce the effective carrier transport pathways and increase the series resistance, thus leading to the deterioration of J_{sc},[67,68] while some argued that voids have no influence on the performance of devices.[69] In this work, it is possible to assume that the voids reduce the effective film thickness, leading to incomplete optical absorption in the back region, correlating with the long wavelength EQE loss and low J_{sc}. Therefore, eliminating voids in CZTSSe devices is necessary for back interface mechanical robustness and efficiency enhancement. In consequence, further processing optimization, e.g., tuning the metallic precursors stacking order, using high chalcogen vapour, and engineering the Mo surface by barrier layers might be possible solutions.[63,70-72]

To sum up, it is of key importance to further optimize the quality of CZTSSe absorbers, by promoting Σ3 type SGBs and reducing secondary phases/inclusions/voids and structural defects such as stacking faults. In addition, the multi-charge character of Sn (IV and II valence state) and volatile nature of Sn chalcogenides could cause secondary phases/voids as well as Sn related deep defects (e.g., Cu_{Sn} and Sn_{Cu}).[14] Thus, a fine tuning of Sn should be taken into serious account.

2.4.2 Back interface (CZTSSe/Mo)

Sulfur rich $Mo(S,Se)_2$ layer with a thickness of less than 100 nm is clearly visible in the back interface (see Figure S8). Nevertheless, although the beneficial effect of $MoSe_2$ that can facilitate an ohmic contact formation has been supported both by experimental results and theoretical simulation in CIGS and CZTSe solar cells,[73-75] the role of $MoS_2/Mo(S,Se)_2$ is still not clearly stated, remaining an open issue to debate. In addition, the optimal thickness of Mo chalcogenides for kesterite/chalcopyrite solar cells is also not clear. It seems that thicknesses in the range of 10-300 nm are somehow suitable. Because absence of $MoSe_2$ interfacial layer will impede the formation of an ohmic contact at the back interface and the back surface recombination will rise quickly. On the contrary, a too thick $MoSe_2$ layer will cause high series resistance.[3,73,76,77] Furthermore, the orientation of Mo chalcogenides is also critical, because Mo chalcogenides have layered structure, thus good carrier transport properties as well as mechanical adhesion can be achieved when the c-axis (perpendicular to the layered planes) is parallel to the substrate while high series resistance and degradation in carrier transport properties are observed when the c-axis is perpendicular to the substrate.[73,78] In the case of our CZTSSe solar cells, the magnified HAADF-STEM image and the corresponding reduced FFT patterns indicate that the species are hexagonal $Mo(S,Se)_2$ monolayers and grow vertically onto the surface of Mo substrate with c-axis parallel to the substrate (see **Figure S10**), which can facilitate carrier transport along the two-dimension (2D) planes of $Mo(S,Se)_2$. However, apart from the detrimental reactions in the back interface CZTSSe/Mo,[65] some fundamental issues, e.g., the band alignment of $CZTSSe/MoS(e)_2$ and the exact back surface recombination rate, are still pending, which requires deeper investigation on both experiments and theory to further optimize the back interface.

3. Conclusions

In summary, in this work we have fabricated the $CZTSSe/Al(OH)_3/CdS$ multi-interfaces using a facile wet chemical treatment based on aluminium chlorides and thioacetamide aqueous

solution. Considerable enhancement of V_{oc} and FF, and ultimately the performance improvement of CZTSSe solar cells are observed. A champion device of 9.1 % efficiency with FF nearly 70 % for a Se-rich CZTSSe solar cell is achieved via systematic optimization of AT chemical treatment. The impact of this AT interface engineering can be explained by: (1) V_{oc} increase is mainly associated to less interface recombination by aluminium hydroxide nanolayers passivation. In addition, the increased surface band gap and carrier concentration could also be partially responsible for the V_{oc} enhancement; (2) FF increment is ascribed to lower series resistance and higher shunt resistance, which are further related to increased carrier concentration and reduced shunt paths; (3) Unaffected J_{sc} is illustrated by higher EQE in the short wavelength region near p-n junction while lower EQE for photogenerated carriers deeper in the absorber, and thereby it is respectively ascribed to better p-n junction quality and shorter effective collection length. The AT chemical treatment strategy in this work paves the way to reduce interface recombination and V_{oc} and FF deficit, which may lead to further efficiency enhancement in the CZTSSe field. Furthermore, taking into account the thermal stability (stable below 300℃) of gibbsite (monoclinic γ-$Al(OH)_3$) and its epitaxial relationship with kesterite and CdS, gibbsite may also be applicable to other thin film photovoltaics, like CdTe, Cu_2SnS_3, $CuSbSe_2$ and Sb_2Se_3 etc., which are using CdS to construct the p-n hetero-junction. Finally, the relevance of improving the quality of the bulk by minimizing structural defects like detrimental GBs and stacking faults and also secondary phases/inclusions/voids, is discussed, which may provide useful information for the community to further improve kesterite solar cell efficiency.

4. Experimental Section

Preparation of absorbers

CZTSSe thin films (Zn/Sn = 1.2-1.25, Cu/(Zn+Sn) = 0.75-0.8 and S/(S+Se) = 0.24-0.3) were prepared by a single-step sulfo-selenization of Cu/Sn/Cu/Zn metallic stack precursors onto

Mo coated soda-lime glass substrates. The singe-step sulfo-selenization was conducted in a graphite box using a two-step thermal profile: first 200 ℃ for 15 min under 1mbar and then 550 ℃ for 30 min under 1bar atmosphere. Se (48 mg) and S (2 mg) as well as Sn (5 mg) were included in the graphite box at the same time. Details of the metallic precursor preparation and the thermal process can be found in our previous works.[79,80] The as-prepared absorbers were subjected to a post low temperature treatment (PLTT) at 300℃ in air for 10 min, with the aim of obtaining better Na spatial distribution in the active interface region.[81]

Chemical treatments and fabrication of solar cells

The as-PLTT absorbers were etched in $(NH_4)_2S$ solution (22% w/w) at room temperature for 2 min to remove Sn(S,Se) secondary phases,[19] and then were immersed in an aqueous solution at 80 ℃ for soaking times ranging from 10 s to 5 min. The aqueous solution is formed by mixing equal volume of aluminum chloride ($AlCl_3$, 0.005-0.1 M)(Alfa Aesar, anhydrous, 99.999 % (metals basis)) and thioacetamide (CH_3CSNH_2, 0.1-0.5 M)(SIGMA-ALDRICH, ACS reagent, ≥ 99.0 %). Immediately after, solar cells were completed by chemical bath deposition (CBD) of 50-70 nm CdS and DC sputtering of 300 nm i-ZnO/ITO window layers sequentially performed onto the chemical treated absorbers.

Characterizations

3×3 mm^2 solar cells were scribed and illuminated and dark current-voltage (J-V) curves were measured using ABET3000 Solar Simulator calibrated with a reference Si solar cell. The external quantum efficiency (EQE) spectra were collected by Bentham PVE300 characterization system calibrated with standard silicon and germanium photodetectors. X-ray diffraction (XRD) (Siemens D500 diffractometer) and scanning electron microscope (SEM) (ZEISS Series Auriga microscope) were employed to investigate the structure and morphology of CZTSSe absorbers. X-ray photoelectron spectroscopy (XPS) measurements were performed in a PHI 5500 Multitechnique System (from Physical Electronics) with a

monochromatic X-ray source (Aluminium Kα line of 1486.6 eV and 350 W), placed perpendicular to the analyzer axis and calibrated using the 3d5/2 line of Ag with a full width at half maximum (FWHM) of 0.8 eV. The analyzed area was a circle of 0.8 mm diameter, and the selected resolution for the spectra was 187.85 eV of Pass Energy and 0.8 eV/step for the general spectra and 23.5 eV of Pass Energy and 0.1 eV/step for the spectra of the different elements. A low energy electron gun (less than 10 eV) was used in order to discharge the surface when necessary. All measurements were made in an ultra-high vacuum (UHV) chamber with pressure between 5×10^{-9} and 2×10^{-8} torr. Capacitance-Voltage (C-V) measurements were performed by using an impedance analyzer from Novocontrol Technologies with a frequency of 15 kHz and a modulation voltage of 50 mV in the dark at room temperature. Temperature dependence of J-V measurements (JV-T) were performed by a Keithley 2400 source meter using a closed-cycle He cryostat (ColdEdge). The illumination source was from a small area Newport solar simulator under AM1.5G light conditions calibrated to one sun by using a Si reference cell. The photoluminescence (PL) spectra were measured using the iHR320 Horiba Jobin Yvon spectrometer coupled with InGaAs detector and He-Ne gas laser with a 632.8 nm laser line used as excitation source. Spectra were measured in backscattering configuration through the Olympus metallographic objective and using the maximum laser power while ensuring the absence of the thermal effects on the samples at the same time. Sample temperature was varied in the close-circle He cryostat and measured by Si-diode. High Resolution Transmission Electron Microscopy (HRTEM) measurements were obtained by using a FEI Tecnai F20 field emission gun microscope operated at 200 kV with a point-to-point resolution of 0.19 nm, which is equipped with a high-angle annular dark field (HAADF) detector. The atomic resolution aberration corrected high angle annular dark field scanning transmission electron microscopy (HAADF-STEM) images were obtained by using a probe corrected FEI Titan 60-300 equipped with a high brightness field emission gun (XFEG) and a CETCOR corrector from CEOS, producing a

probe size of about 0.8 Å. The microscope was operated at 300 kV, with a convergence angle of 23 mrad and an inner collection angle of the detector of 62 mrad. A Wiener and 4th order Gaussian background subtracted filter were applied to the atomic HAADF-STEM images by using the software STEM-CELL.[82-84]

Supporting Information

Supporting Information is available from the Wiley Online Library or from the author.

Acknowledgements

The authors thank Dr. Florian Oliva for experimental and characterization assistance. The research leading to these results has received funding from Generalitat de Catalunya 2014SGR1638 and the Spanish MINECO (Ministerio de Economía y Competitividad de España) under the NASCENT (ENE2014-56237-C4-1-R), the TNT-FUELS and e-TNT (MAT2014-59961) projects, funding from the Framework 7 program under the project KESTCELLS (FP7-PEOPLE-2012-ITN-316488) and European Regional Development Founds (ERDF, FEDER Programa Competitivitat de Catalunya 2007–2013). Authors from IREC and IN2UB belong to the M-2E (Electronic Materials for Energy) Consolidated Research Group and the XaRMAE Network of Excellence on Materials for Energy of the "Generalitat de Catalunya". H. Xie thanks the "China Scholarship Council" fellowship (CSC Nº201206340113), Y. S. the MINECO for the PTA fellowship (PTA2012-7852-A), and E.S. the "Ramon y Cajal" fellowship (RYC-2011-09212). ICN2 acknowledges support from the Severo Ochoa Program (MINECO, Grant SEV-2013-0295). Part of the present work has been performed in the framework of Universitat Autònoma de Barcelona Materials Science Ph.D. program.

Received: ((will be filled in by the editorial staff))
Revised: ((will be filled in by the editorial staff))
Published online: ((will be filled in by the editorial staff))

References

[1] D. B. Mitzi, O. Gunawan, T. K. Todorov, K. Wang, S. Guha, *Sol. Energy Mater. Sol. Cells* **2011**, *95*, 1421.

[2] A. Zuser, H. Rechberger, *Resour., Conserv. Recycl.***2011**, *56*, 56.

[3] W. Wang, M. T. Winkler, O. Gunawan, T. Gokmen, T. K. Todorov, Y. Zhu, D. B. Mitzi, *Adv.Energy Mater.* **2014**, *4*, 1301465.

[4] https://www.nrel.gov/pv/assets/pdfs/pv-efficiencies-07-17-2018.pdf.

[5] S. Giraldo, M. Neuschitzer, T. Thersleff, S. López-Marino, Y. Sánchez, H. Xie, M. Colina, M.Placidi, P. Pistor, V. Izquierdo-Roca, K. Leifer, A. Pérez-Rodríguez , E. Saucedo, *Adv. Energy Mater.* **2015**, *5*, 1501070.

[6] S. G. Haass, M. Diethelm, M. Werner, B. Bissig, Y. E. Romanyuk, A. N. Tiwari, *Adv. Energy Mater.* **2015**, *5*, 1500712.

[7] P. Jackson, R. Wuerz, D. Hariskos, E. Lotter, W. Witte, M. Powalla, *Phys. Status Solidi RRL* **2016**, *10*, 583.

[8] A. Chirilă, P. Reinhard, F. Pianezzi, P. Bloesch, A. R. Uhl, C. Fella, L. Kranz, D. Keller, C. Gretener, H. Hagendorfer, D. Jaeger, R. Erni, S. Nishiwaki, S. Buecheler , A. N. Tiwari, *Nat. Mater.* **2013**, *12*, 1107.

[9] T. Gokmen, O. Gunawan, T. K. Todorov , D. B. Mitzi, *Appl. Phys. Lett.* **2013**, *103*, 103506.

[10] G. Rey, G. Larramona, S. Bourdais, C. Chone, B. Delatouche, A. Jacob, G. Dennler, S. Siebentritt, *Sol. Energy Mater. Sol. Cells* **2018**, *179*, 142.

[11] Y. S. Lee, T. Gershon, O. Gunawan, T. K. Todorov, T. Gokmen, Y. Virgus, S. Guha, *Adv. Energy Mater.* **2015**, *5*, 1401372.

[12] M. G. Gang, S. W. Shin, M. P. Suryawanshi, U. V. Ghorpade, Z. Song, J. S. Jang, J. H. Yun, H. Cheong, Y. Yan, J. H. Kim, *J. Phys. Chem. Lett.***2018**, *9*, 4555.

[13] G. Oki, K. T. Teodor, B. M. David, *Appl. Phys. Lett.* **2010**, *97*, 233506.

[14] G. Larramona, S. Levcenko, S. Bourdais, A. Jacob, C. Chon é, B. Delatouche, C. Moisan, J. Just, T. Unold, G. Dennler, *Adv. Energy Mater.* **2015**, *5*, 1501404.

[15] C. Yan, J. Huang, K. Sun, S. Johnston, Y. Zhang, H. Sun, A. Pu, M. He, F. Liu, K. Eder, L. Yang, J. M. Cairney, N. J. Ekins-Daukes, Z. Hameiri, J. A. Stride, S. Chen, M. A. Green, X. Hao, *Nat. Energy* **2018**, *3*, 764.

[16] T. Shin, I. Tadayoshi, H. Hirofumi, O. Keiichiro, A. Ryoji, *Appl. Phys. Express* **2015**, *8*, 082302.

[17] C. Yan, Fangyang Liu, Ning Song , Boon K. Ng, John A. Stride, Anton Tadich, and Xiaojing Hao, *Appl. Phys. Lett.* **2014**, *104*, 173901.

[18] M. Bar, B. A. Schubert, B. Marsen, R. G. Wilks, S. Pookpanratana, M. Blum, S. Krause, T. Unold, W. Yang, L. Weinhardt, C. Heske, H. W. Schock, *Appl. Phys. Lett.* **2011**, *99*, 222105.

[19] K. Sun, C. Yan, F. Liu, J. Huang, F. Zhou, J. A. Stride, M. Green, X. Hao, *Adv. Energy Mater.* 2016, 6, 1600046.

[20] H. Xie, Y. S ánchez, S. L ópez-Marino, M. Esp índola-Rodr guez, M. Neuschitzer, D. Sylla, A. Fairbrother, V. Izquierdo-Roca, A. P érez-Rodr guez, E. Saucedo, *ACS Appl. Mater. Interfaces* **2014**, *6*, 12744.

[21] S. L ópez-Marino, Y. S ánchez, M. Placidi, A. Fairbrother, M. Espindola-Rodr guez, X. Fontan é, V. Izquierdo-Roca, J. L ópez-Garc á, L. Calvo-Barrio, A. P érez-Rodr guez, E. Saucedo, *Chem. – Eur. J.***2013**, *19*, 14814.

[22] F. Liu, C. Yan, J. Huang, K. Sun, F. Zhou, J. A. Stride, M. A. Green, X. Hao, *Adv. Energy Mater.* **2016**, *6*, 1600706.

[23] Y. S ánchez, M. Esp índola-Rodr guez, H. Xie, S. L ópez-Marino, M. Neuschitzer, S. Giraldo, M. Dimitrievska, M. Placidi, V. Izquierdo-Roca, F. A. Pulgar ín-Agudelo, O. Vigil-Gal án, E. Saucedo, *Sol. Energy Mater. Sol. Cells* **2016**, *158, Part 2*, 138.

[24] J. M. Ball, M. M. Lee, A. Hey, H. J. Snaith, *Energy Environ. Sci.* 2013, *6*, 1739.

[25] O. Kunz, J. Wong, J. Janssens, J. Bauer, O. Breitenstein, A. G. Aberle, *Prog. Photovoltaics* 2009, *17*, 35.

[26] D. Lausch, V. Naumann, A. Graff, A. Hähnel, O. Breitenstein, C. Hagendorf, J. Bagdahn, *Energy Procedia* 2014, *55*, 486.

[27] J. Schmidt, A. Merkle, R. Brendel, B. Hoex, M. C. M. v. de Sanden, W. M. M. Kessels, *Prog. Photovoltaics* 2008, *16*, 461.

[28] W. Wu, Y. Cao, J. V. Caspar, Q. Guo, L. K. Johnson, R. S. McLean, I. Malajovich, K. R. Choudhury, *Appl. Phys. Lett.* 2014, *105*, 042108.

[29] Y. S. Lee, T. Gershon, T. K. Todorov, W. Wang, M. T. Winkler, M. Hopstaken, O. Gunawan, J. Kim, *Adv. Energy Mater.*2016, *6*, 1600198.

[30] T. Nakada, K. Matsumoto, M. Okumura, presented at *Proc. 29th IEEE Photovoltaic Specialists Conf. (PVSC)*, New Orleans, LA, May 2002.

[31] C.-W. Chen, H.-W. Tsai, T.-T. Wu, Y.-T. Yen, Y.-C. Wang, C.-H. Hsu, W.-C. Tsai, H.-S. Tsai, C.-H. Shen, J.-M. Shieh, Y.-L. Chueh, *J. Mater. Chem. A* 2015, *3*, 14985.

[32] W.-H. Ho, C.-H. Hsu, T.-H. Yeh, Y.-H. Chang, S.-Y. Wei, T.-Y. Lin, C.-H. Lai, *ACS Appl. Mater. Interfaces* 2016, *8*, 6709.

[33] E. Wiberg, N. Wiberg, A F Holleman, *Inorganic Chemistry*, Academic Press, Berlin, Germany 2001.

[34] W. Hummel, U. Berner, E. Curti, F. J. Pearson, T. Thoenen, *Nagra/PSI Chemical Thermodynamic Data Base 01/01*, Universal Publishers, Boca Raton, FL, USA 2002.

[35] C. Jianfei, W. Xin, X. Yinghong, W. Xiaodong, Z. Li, Y. Wei, *Nanotechnol.* 2007, *18*, 135706.

[36] J. Kim, H. Hiroi, T. K. Todorov, O. Gunawan, M. Kuwahara, T. Gokmen, D. Nair, M. Hopstaken, B. Shin, Y. S. Lee, W. Wang, H. Sugimoto, D. B. Mitzi, *Adv. Mater.* 2014, *26*, 7427 – 7431.

[37] S. S. Hegedus, W. N. Shafarman, *Prog. Photovoltaics* **2004**, *12*, 155.

[38] S. Levcenko, J. Just, A. Redinger, G. Larramona, S. Bourdais, G. Dennler, A. Jacob, T. Unold, *Phys. Rev. Appl.* **2016**, *5*, 024004.

[39] X. Lin, A. Ennaoui, S. Levcenko, T. Dittrich, J. Kavalakkatt, S. Kretzschmar, T. Unold, M. C. Lux-Steiner, *Appl. Phys. Lett.* **2015**, *106*, 013903.

[40] W. E. Dubbin, G. Sposito, M. Zavarin, *Soil Sci.* **2000**, *165*, 699.

[41]J. Frenzel1, A. F. Oliveira, H. A. Duarte, Zeitschrift für anorganische und allgemeine Chemie, **2005**, *631*, 1267–1271.

[42] K. G. Deepa, N. Lakshmi Shruthi, M. Anantha Sunil, J. Nagaraju, *Thin Solid Films* **2014**, *551*, 1 – 7.

[43] H. Wei-Chih, X. Zeng, W. Shih-Yuan, C. Chung-Hao, L. Tzu-Ying, L. H. Wong, L. Chih-Huang, *Proc. IEEE 42th Photovoltaic Specialists Conf. PVSC* **2015**, 1 – 4.

[44] J. H. Kim, S.-Y. Choi, M. Choi, T. Gershon, Y. S. Lee, W. Wang, B. Shin, S.-Y. Chung, *Adv. Energy Mater.* **2016**, *6*, 1501902.

[45] G. Niu, W. Li, F. Meng, L. Wang, H. Dong, Y. Qiu, *J. Mater. Chem. A* **2014**, *2*, 705-710.

[46]. Whittington, D. Ilievski, *Chem. Eng. J.* **2004**, *98*, 89 – 97.

[47] P. Cees W. , T. Rudolph A. J. , *Microtectonics*, Springer, Berlin, Germany **2005**.

[48] D. Abou-Ras, S. Schorr, H. W. Schock, *J. Appl. Crystallogr.* **2007**, *40*, 841.

[49] D. Abou-Ras, C. T. Koch, V. Küstner, P. A. van Aken, U. Jahn, M. A. Contreras, R. Caballero, C. A. Kaufmann, R. Scheer, T. Unold, H. W. Schock, *Thin Solid Films* **2009**, *517*, 2545.

[50] C. L. Johnson, E. Snoeck, M. Ezcurdia, B. Rodriguez-Gonzalez, I. Pastoriza-Santos, L. M. Liz-Marzan, M. J. Hytch, *Nat. Mater.* **2008**, *7*, 120.

[51] C. K. Miskin, W.-C. Yang, C. J. Hages, N. J. Carter, C. S. Joglekar, E. A. Stach, R. Agrawal, *Prog. Photovoltaics* **2015**, *23*, 654.

[52] S. Chen, A. Walsh, X.-G. Gong, S.-H. Wei, Adv. Mater. 2013, 25, 1522.

[53] V. Naumann, D. Lausch, A. Hähnel, J. Bauer, O. Breitenstein, A. Graff, M. Werner, S. Swatek, S. Großer, J. Bagdahn, C. Hagendorf, *Sol. Energy Mater. Sol. Cells* **2014**, *120*, 383.

[54] I.D. Olekseyuk, I.V. Dudchak, L.V. Piskach, *J. Alloys Compd.* **2004**, *368*, 135.

[55] I. V. Dudchak, L. V. Piskach, *J. Alloys Compd.* **2003**, *351*, 145.

[56] A. Fairbrother, M. Dimitrievska, Y. Sanchez, V. Izquierdo-Roca, A. Perez-Rodriguez, E. Saucedo, *J. Mater. Chem. A* **2012**, *3*, 9451.

[57] H. Katagiri, K. Jimbo, M. Tahara, H. Araki, K. Oishi, *MRS Proc.* **2009**, *1165*, 1165-M04-01.

[58] Q. Cao, O. Gunawan, M. Copel, K. B. Reuter, S. J. Chey, V. R. Deline, D. B. Mitzi, *Adv. Energy Mater.* **2011**, *1*, 845.

[59] C. H. Lei, A. A. Rockett, I. M. Robertson, N. Papathanasiou, S. Siebentritt, *J. Appl. Phys.* **2006**, *100*, 114915.

[60] G. Brammertz, M. Buffière, S. Oueslati, H. ElAnzeery, K. Ben Messaoud, S. Sahayaraj, C. Köble, M. Meuris, J. Poortmans, *Appl. Phys. Lett.* **2013**, *103*,163904.

[61] F. Zhou, F. Zeng, X. Liu, F. Liu, N. Song, C. Yan, A. Pu, J. Park, K. Sun, X. Hao, *ACS Appl. Mater. Interfaces* **2015**, *7*, 22868.

[62] Z. Rui, R. H. Dennis, K. Jerzy, *Jpn. J. Appl. Phys.* **2013**, *52*, 092302.

[63] H. Araki, A. Mikaduki, Y. Kubo, T. Sato, K. Jimbo, W. S. Maw, H. Katagiri, M. Yamazaki, K. Oishi, A. Takeuchi, *Thin Solid Films* **2008**, *517*, 1457.

[64] H. Cui, W. Li, X. Liu, N. Song, C.-Y. Lee, F. Liu, X. Hao, *Appl. Phys. A* **2015**, *118*, 893.

[65] J. J. Scragg, J. T. Wätjen, M. Edoff, T. Ericson, T. Kubart, C. Platzer-Björkman, *J. Am. Chem. Soc.* **2012**, *134*, 19330.

[66] A. Fairbrother, X. Fontané, V. Izquierdo-Roca, M. Placidi, D. Sylla, M. Espindola-Rodriguez, S. López-Mariño, F. A. Pulgarín, O. Vigil-Galán, A. Pérez-Rodríguez, E. Saucedo, *Prog. Photovoltaics* **2014**, *22*, 479.

[67] W. Li, J. Chen, H. Cui, F. Liu, X. Hao, *Mater. Lett.* **2014**, *130*, 87.

[68] C.-Y. Peng, T. P. Dhakal, S. Garner, P. Cimo, S. Lu, C. R. Westgate, *Thin Solid Films* **2014**, *562*, 574.

[69] H. Flammersberger, *Doctor Thesis*, Uppsala University, December, **2010**.

[70] A. Redinger, D. M. Berg, P. J. Dale, S. Siebentritt, *J. Am. Chem. Soc.* **2011**, *133*, 3320.

[71] Y. Ren, N. Ross, J. K. Larsen, K. Rudisch, J. J. S. Scragg, C. Platzer-Bjorkman, *Chemistry of Materials* **2017**, *29*, 3713.

[72] S. Lopez-Marino, M. Placidi, A. Perez-Tomas, J. Llobet, V. Izquierdo-Roca, X. Fontane, A. Fairbrother, M. Espindola-Rodriguez, D. Sylla, A. Perez-Rodriguez, E. Saucedo, *J. Mater. Chem. A* **2013**, *1*, 8338.

[73] S. Lopez-Marino, M. Espíndola-Rodríguez, Y. Sánchez, X. Alcobé, F. Oliva, H. Xie, M. Neuschitzer, S. Giraldo, M. Placidi, R. Caballero, V. Izquierdo-Roca, A. Pérez-Rodríguez, E. Saucedo, *Nano Energy* **2016**, *26*, 708.

[74] D. Cozza, C. M. Ruiz, D. Duch, J. J. Simon, L. Escoubas, *IEEE J. Photovoltaics* **2016**, *6*, 1292.

[75] D. Abou-Ras, G. Kostorz, D. Bremaud, M. Kälin, F. V. Kurdesau, A. N. Tiwari, M. Döbeli, *Thin Solid Films* **2005**, *480-481*, 433.

[76] B. Shin, Y. Zhu, N. A. Bojarczuk, S. Jay Chey, S. Guha, *Appl. Phys. Lett.* **2012**, *101*, 053903.

[77] J. Li, Y. Zhang, W. Zhao, D. Nam, H. Cheong, L. Wu, Z. Zhou, Y. Sun, *Adv. Energy Mater.* **2015**, *5*, 1402178.

[78] C. M. Ruiz, A. Pérez-Rodríguez, J. Arbiol, J. R. Morante, V. Bermúdez, *Phys. Status Solidi A* **2015**, *212*, 61.

[79] H. Xie, M. Dimitrievska, X. Fontané, Y. Sánchez, S. López-Marino, V. Izquierdo-Roca, V. Bermúdez, A. Pérez-Rodríguez, E. Saucedo, *Sol. Energy Mater. Sol. Cells* **2015**, *140*, 289.

[80] A. Fairbrother, X. Fontané, V. Izquierdo-Roca, M. Espindola-Rodriguez, S. López-Marino, M. Placidi, J. López-García, A. Pérez-Rodríguez, E. Saucedo, *ChemPhysChem* **2013**, *14*, 1836.

[81] H. Xie, S. López-Marino, T. Olar, Y. Sánchez, M. Neuschitzer, F. Oliva, S. Giraldo, V. Izquierdo-Roca, I. Lauermann, A. Pérez-Rodríguez, E. Saucedo, *ACS Appl. Mater. Interfaces* **2016**, *8*, 5017.

[82] V. Grillo, *Microsc. Microanal.* **2011**, *17*, 1292.

[83] V. Grillo, E. Rotunno, *Ultramicroscopy* **2013**, *125*, 97.

[84] V. Grillo, F. Rossi, *Ultramicroscopy* **2013**, *125*, 112.

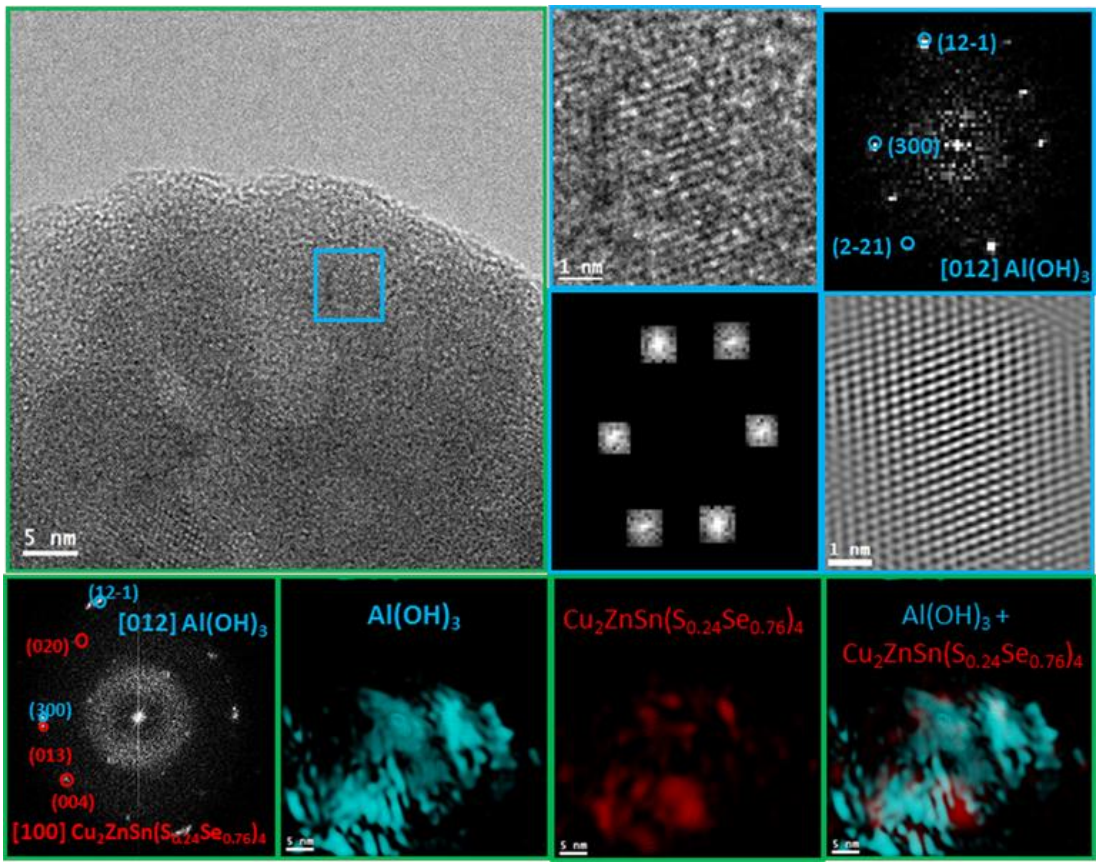

Figure 1. Top row (left): HRTEM micrograph of one representative CZTSSe absorber nanoparticle (dispersed in hexane) after AT treatment (60s). Top row (right): The magnified HRTEM image of the indigo squared area; the corresponding reduced FFT patterns indicate that the species is monoclinic γ-$Al(OH)_3$ (Gibbsite), [P121/N1]-space group 14, with lattice parameters of a = 0.86676 nm, b = 0.50741 nm, c = 0.9728 nm, and α = 90°, β = 94.54°, γ = 90 °as visualized along the [012] direction; the spot mask filtered reduced FFT and the IFFT image. Bottom row: the reduced FFT of the whole HRTEM image, the IFFT of $Al(OH)_3$ (indigo), $Cu_2ZnSn(S_{0.24}Se_{0.76})_4$ (red) and their Red-Green-Blue (RGB) composite.

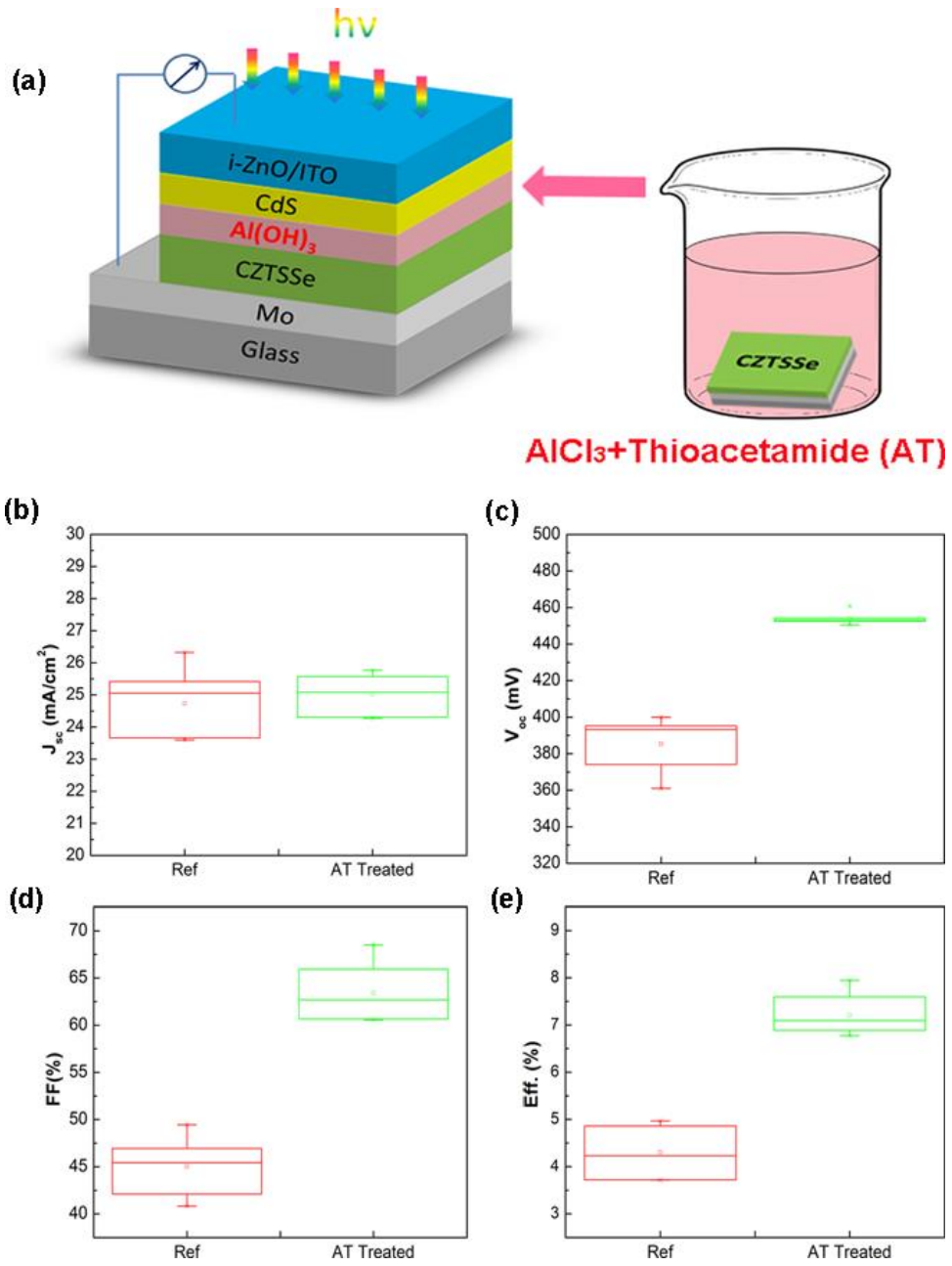

Figure 2. Schematic of the AT treatment and the device architecture of CZTSSe solar cells (a), and optoelectronic parameters of CZTSSe solar cells before and after AT treatment: J_{sc} (b), V_{oc} (c) , FF (d) and Eff. (e). More than 7 cells were included in each group.

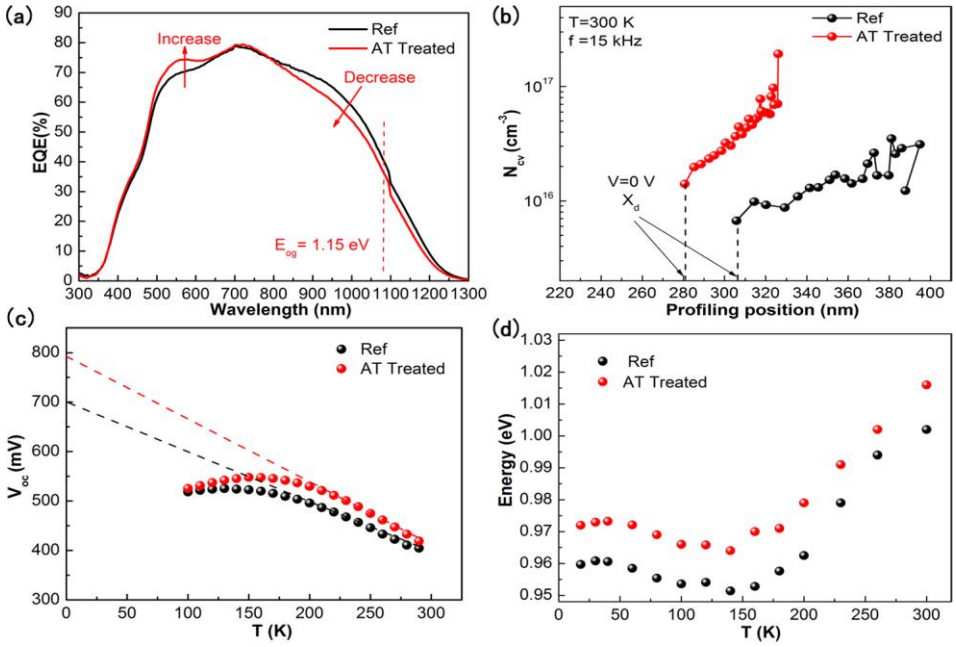

Figure 3. EQE (a), C-V (b), temperature dependence of V_{oc} (c) and PL band maximum position (d) measurements of the reference and AT treated devices.

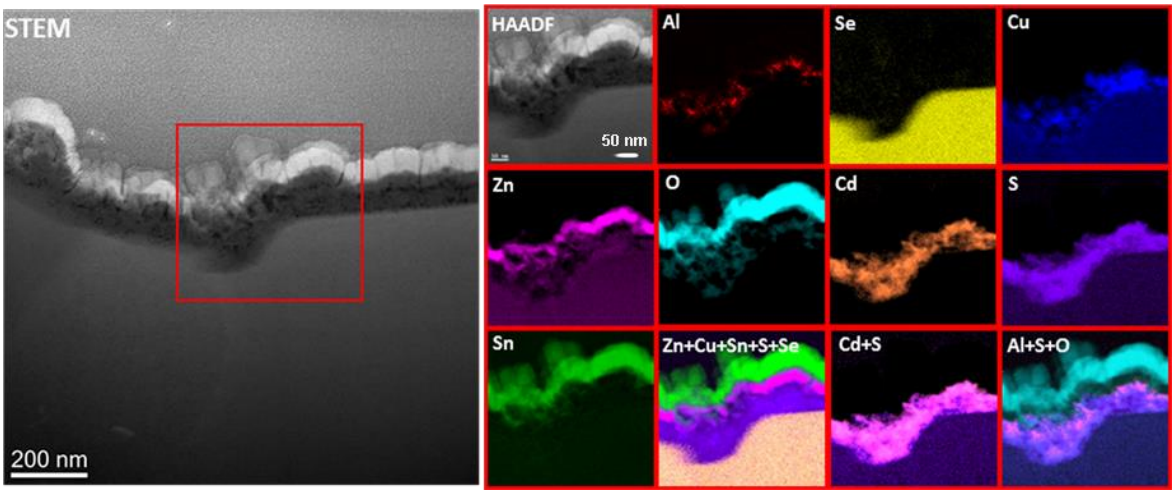

Figure 4. EELS chemical composition maps obtained from the red rectangle area (CZTSSe/CdS interface region) of the HAADF-STEM micrograph of an AT treated device. Individual Al (red), Se (yellow), Cu (blue), Zn (pink), O (indigo), Cd (orange), S (purple), Sn (green) maps and their composite are presented (dual scan, collection time: 50ms/pixel, energy dispersion: 0.7 eV/channel).

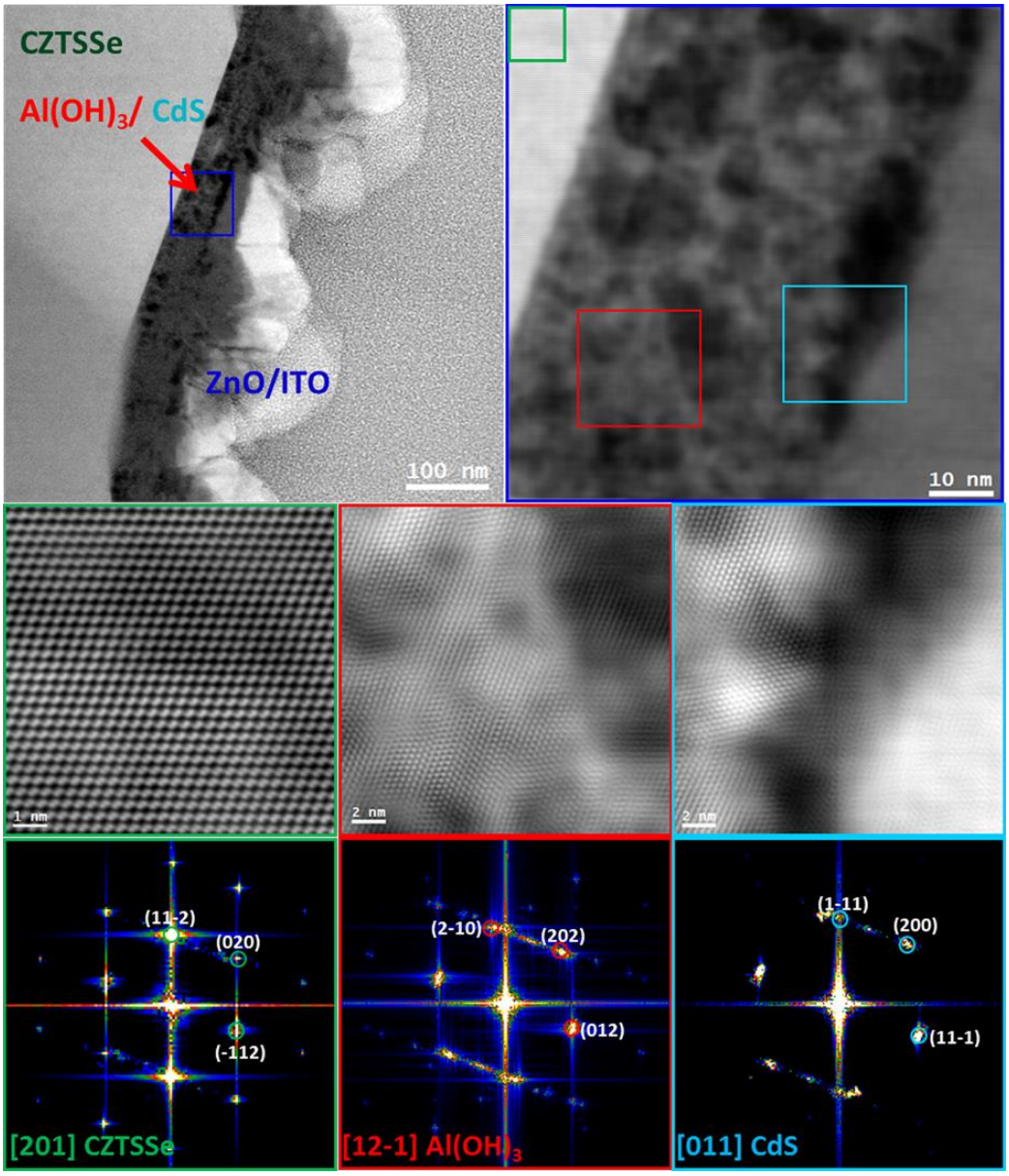

Figure 5. Atomic resolution HAADF-STEM images and corresponding FFT patterns of the CZTSSe/$Al(OH)_3$/CdS interface region in an AT treated device, showing an epitaxial relationship of $Al(OH)_3$ with CZTSSe and CdS.

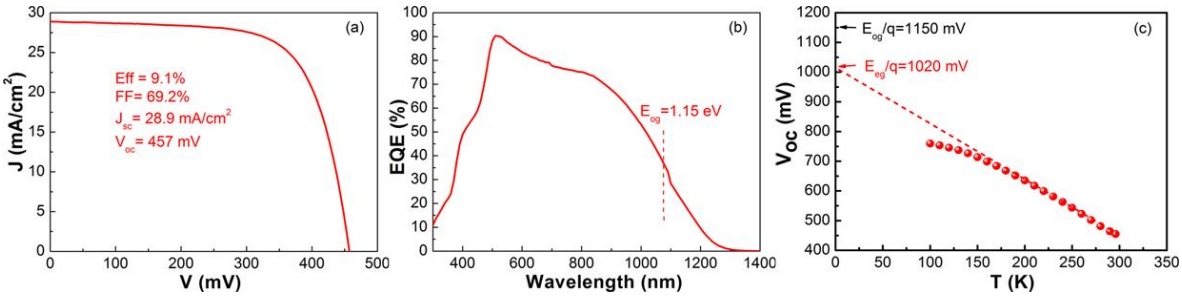

Figure 6. J-V curve (a), EQE plot (b) and temperature dependence of V_{oc} measurement (c) of the 9.1 % champion Se-rich CZTSSe solar cell.

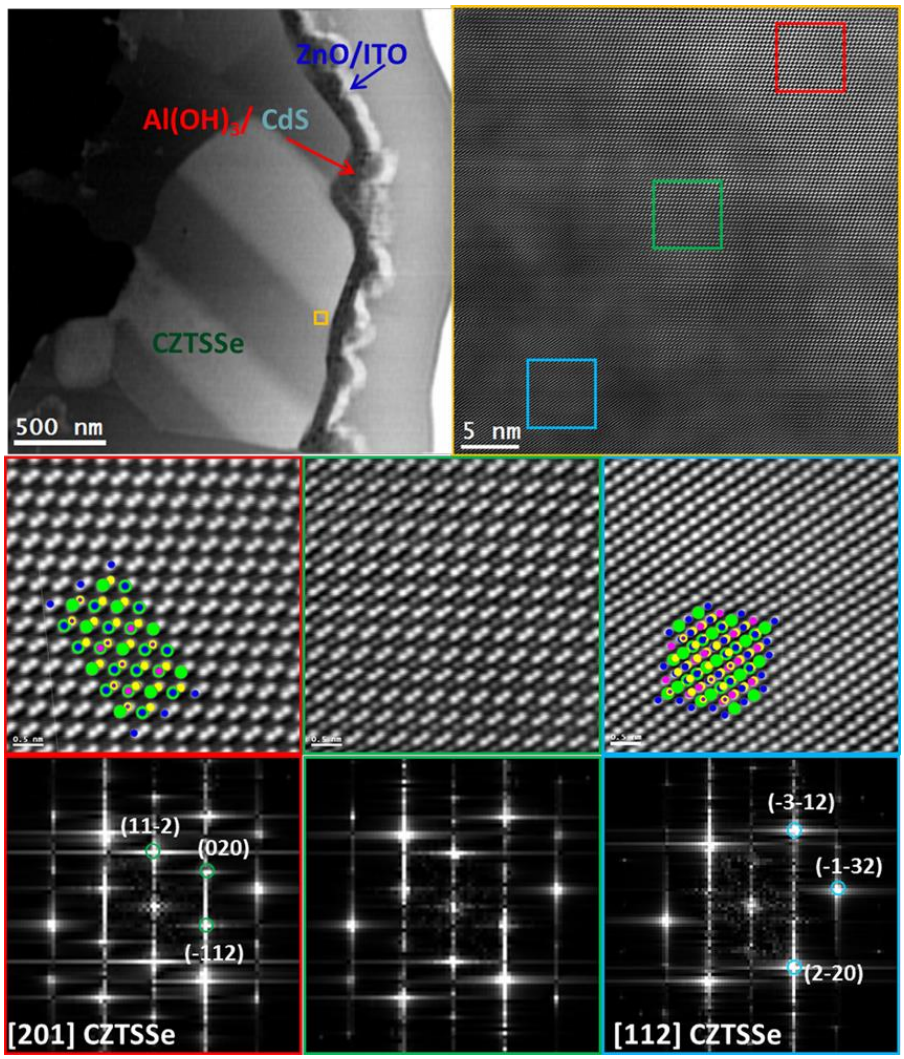

Figure 7. Top row: general HAADF-STEM view of straight grain boundaries (SGBs) present at the CZTSSe matrix of the 9.1% device. Middle row: the atomic resolution HAADF-STEM of different selected squared areas. Bottom row: the corresponding FFT patterns exhibit diffraction spots change in different analyzed squared regions which result from the different orientations observed on the CZTSSe grains. The middle FFT is showing the overlapping between the two grains at the region of the grain boundary (GB).

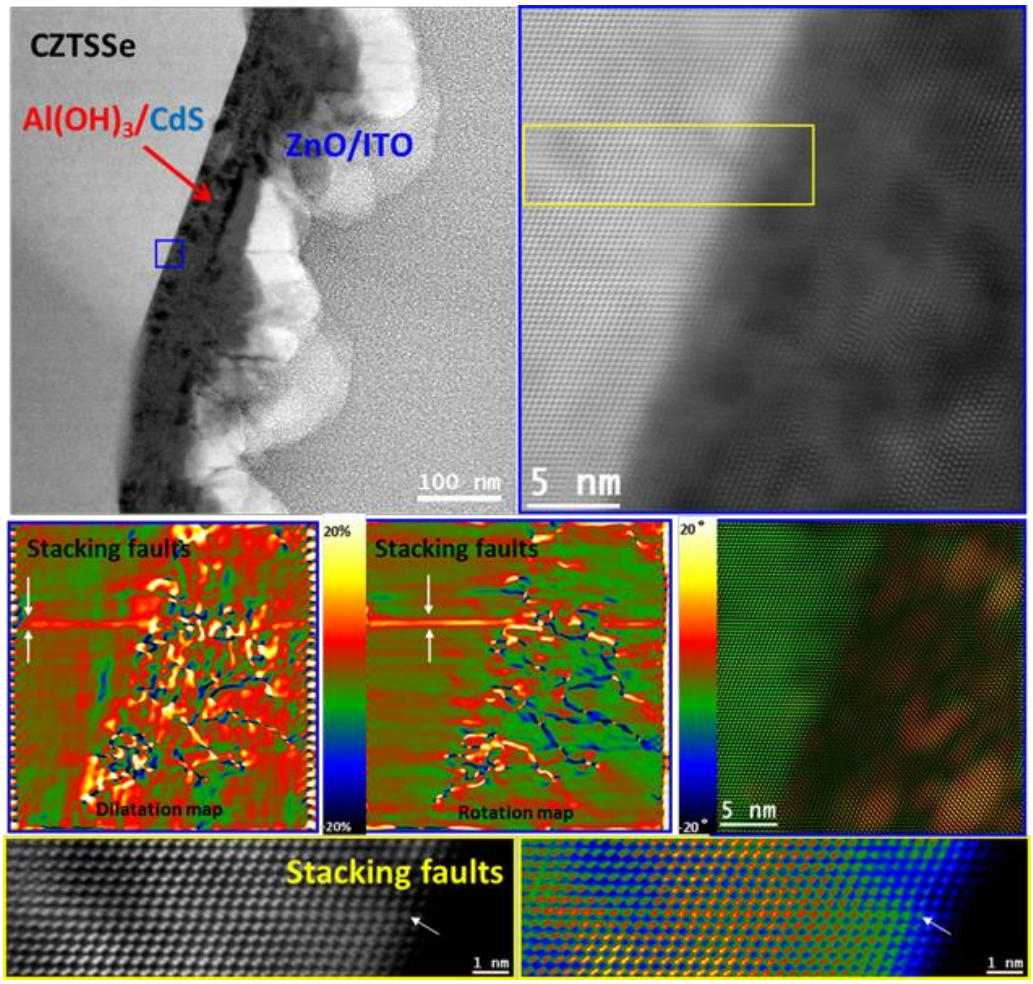

Figure 8. Top row: general view of the front interface areas and the magnified HAADF-STEM image of the blue squared area. Middle row (left): the corresponding dilatation map (+9.8% deformation) and rotation map (+9.5 °rotation) via GPA based on (020) planes of CZTSSe reflections confirm the presence of stacking faults in the CZTSSe matrix area of the 9.1% device, as indicated by the white rows in the magnified HAADF-STEM images of the yellow squared area (bottom row). Middle row (right): IFFT RGB composite of CZTSSe (green) and $Al(OH)_3$ (red) species.

Table 1. Diode analysis of CZTSSe solar cells before and after AT treatment.

	E_{og} (eV)	Φ_b (eV)	J_{sc} ($mA.cm^{-2}$)	V_{oc} (mV)	FF (%)	Eff. (%)	R_s ($\Omega.cm^2$)	R_{sh} ($\Omega.cm^2$)	J_0 ($mA.cm^{-2}$)	A
Ref	1.15	0.7	25.4	395	49.4	5	1.5	104	2.9×10^{-3}	1.65
AT Treated	1.15	0.8	25.6	453	68.5	7.9	0.7	550	1.9×10^{-4}	1.47